Journal of the Serbian Chemical Society
JSCS@tmf.bg.ac.rs • www.shd.org.rs/JSCS

J. Serb. Chem. Soc. 90 (4) 497–511 (2025)
JSCS–5402

Original scientific paper
Published 24 April, 2025

Modification of surface properties and photocatalytic performance of pure and oxygen-doped graphitic carbon nitride *via* DBD plasma treatment

JANA LJ. PETROVIĆ[1]*, ŽELJKO RADOVANOVIĆ[1], BRATISLAV OBRADOVIĆ[2], ĐORĐE JANAĆKOVIĆ[3] and RADA PETROVIĆ[3]

[1]*Innovation Center of the Faculty of Technology and Metallurgy, Ltd, Belgrade, Serbia,* [2]*University of Belgrade, Faculty of Physics, Belgrade, Serbia and* [3]*University of Belgrade, Faculty of Technology and Metallurgy, Belgrade, Serbia*

(Received 10 November, revised 19 November 2024, accepted 10 January 2025)

Abstract: Graphitic carbon nitride (CN) is a non-metallic semiconductor with applications in photocatalysis, including the photocatalytic reduction of Cr(VI) under visible irradiation. To improve its intrinsic properties, two modification strategies were applied: *i*) oxygen doping by co-calcination of urea with two different amounts of oxalic acid and *ii*) dielectric barrier discharge (DBD) plasma treatment. The plasma treatment was applied to pristine and previously oxygen-doped CNs. The properties of the photocatalysts were studied by XRD, FTIR, FESEM, EDS, PL and DRS analysis, as well as by determination of the number of acidic surface functional groups. Both modification methods increased the oxygen content: during oxygen doping, nitrogen was replaced by oxygen in the lattice, while during plasma treatment, oxygen-containing functional groups were introduced at the surface. Plasma treatment of oxygen-doped CNs facilitated surface functionalisation due to the open heptazine ring structure. Oxygen doping narrowed the band gap, which was further slightly reduced by subsequent plasma treatment, thereby lowering the oxidation and reduction potentials. Although the absorption of visible light was improved, the reduction of the band gap resulted in a reduced activity for the photocatalytic reduction of Cr(VI). The best results were obtained with plasma-treated pure CN, due to the increased content of oxygen-containing surface groups, which led to a slightly reduced recombination rate of charge carriers

Keywords: semiconductor; photocatalytic reduction; water treatment; Cr(VI).

* Corresponding author. E-mail: petrovicj@tmf.ac.bg.rs
https://doi.org/10.2298/JSC241110003P

INTRODUCTION

Graphitic carbon nitride (CN) is a unique semiconductor-based photocatalyst, characterised by a graphite-like structure, which has been widely used in many applications such as solar cells or photocatalytic water-splitting, but also in environmental remediation, including photocatalytic reduction of toxic Cr(VI). Numerous advantages, such as a suitable band gap energy (~2.7 eV), high conduction band potential, *i.e.*, high reduction potential of electrons, non-toxicity and resistance to extreme pH conditions, have attracted much attention to CN.[1,2] In addition, CN synthesis is typically achieved by facile direct thermal condensation of nitrogen-rich precursors such as urea, thiourea, melamine, cyanamide, or dicyandiamide. In particular, urea-derived CN has been reported to possess the most favourable properties for Cr(VI) reduction.[3] Nevertheless, bulk CN faces challenges such as high recombination rates of photogenerated charge carriers and low visible light utilization, which limit its photocatalytic efficiency. Numerous modification strategies have been proposed to enhance its photocatalytic activity, such as elemental doping to alter the electronic structure and band gap width, forming heterojunctions with other semiconductors, carbon materials or depositing metal nanoparticles (NPs) on the CN surface to improve the separation of photogenerated electrons and holes.[4] The choice of modification strongly depends on the desired application, so it is advantageous to tailor the photocatalyst to the operating conditions.

In addition to the aforementioned strategies involving the integration of other materials, another effective approach to optimizing CN for photocatalytic reduction involves the introduction of defects and functional group modifications.[5,6] It is well known that surface properties, such as specific surface area, presence of surface functional groups, number of active sites, and surface charge, significantly influence the photocatalytic performance of materials, since photoinduced reactions take place at the surface of the photocatalyst.[7] Functionalization of the CN surface with electron-withdrawing oxygen-containing functional groups, can alter the charge distribution within the CN. It has been reported that this modification enhances the separation and migration of photogenerated charge carriers, prevents their recombination and provides additional active sites on the CN surface.[5,8,9] Furthermore, the introduction of these hydrophilic groups can improve the dispersibility of CN in water, thereby increasing the surface area exposed to Cr(VI) ions for adsorption and facilitating the interactions with radiation necessary for photocatalyst activation.[10–12]

As one of the most promising physical methods, plasma surface modification has been widely used to improve the surface properties of carbon materials by introducing different functional groups and increasing the number of adsorption sites.[13] The type of functional groups introduced depends on the atmosphere used in the plasma treatment. For example, to increase the amount of oxygen-con-

taining functional groups, an air atmosphere is usually used, which further simplifies and economises this method. In addition, plasma treatment of a photocatalyst can alter its electronic structure, increase its hydrophilicity and improve its dispersity, thereby increasing the surface area available for adsorption.[14] In theory, a plasma consists of neutral species, positive ions and electrons, which form an oxidizing medium and can interact with materials to optimize their surface morphology or chemical properties, without destroying the fundamental structure.[15,16] Dielectric barrier discharge (DBD) plasma belongs to the non-thermal plasma (NTP) discharge and has been widely used for material modification due to the its advantages, such as the ability to operate at an atmospheric pressure, low gas temperature, it has uniform discharge and high electron density.[17–19] Mao *et al.* used DBD, at room temperature and atmospheric pressure air without flow, to modify the surface properties of CN.[7] The results showed that the plasma treatment didn't affect the crystal structure of CN, but the crystallinity was reduced. In addition, EDS analysis showed that there was a higher oxygen content and FTIR confirmed that the peak assigned to –OH groups was higher from the pure CN. This probably led to the reduced recombination of electrons and holes. The obtained photocatalyst was investigated for the photocatalytic degradation of Rhodamine B (RhB) under visible irradiation and its activity was improved compared to the pristine CN.

Plasma treatment can be applied to pure CN, although there is evidence that it may be more effective when applied to pre-treated CN with introduced defects such as dopants or vacancies. The introduction of these defects can lead to the opening of the CN heptazine ring, facilitating the attachment of new functional groups to the "exposed" ends.[20,21] As CN naturally contains some oxygen, it is assumed that doping CN with additional oxygen to increase its content could promote ring opening and facilitate the introduction of carboxyl, carbonyl and hydroxyl groups. It has also been reported that oxygen-doped CN has a narrower band gap and a more porous structure than pure CN, which could further enhance its photocatalytic activity.[22,23]

In this study, DBD plasma treatment was used to modify both pure CN, obtained by thermal polymerisation of urea, and oxygen-doped CN, obtained by co-calcination of urea with oxalic acid. While plasma treatment has previously been used for surface modification of CN, research on its application to oxygen-doped CN remains limited. Furthermore, the influence of the modifications of CN on the photocatalytic reduction of Cr(VI) hasn't been investigated. Therefore, the effects of DBD plasma treatment on the crystallinity, chemical composition, morphology, optical absorption, electronic properties and acidic surface group content, as well as on the Cr(VI) photocatalytic reduction of urea-derived and oxygen-doped CN, were investigated.

EXPERIMENTAL

Direct thermal polymerization of urea (Thermo Fisher Scientific, Germany (99.5%)) was used for the synthesis of bulk CN. An alumina crucible containing urea, covered with a lid, was heated in a muffle furnace in air atmosphere at a heating rate of 10 °C/min to 550 °C and held at this temperature for 4 h. The furnace was cooled to ambient temperature and the resulting yellow sample was ground to powder and collected for further use.

Oxygen-doped CN samples were prepared by the co-calcination method of urea with oxalic acid (OA, oxalic acid dihydrate, Zorka Pharma a. d., Šabac (99.5 %)). 10 g of urea was well ground with a certain amount of oxalic acid (2 or 5 g) in a mortar, transferred to an alumina crucible with a lid and kept in a muffle furnace for 4 h at 550 °C in air. When 2 g of oxalic acid was used, the heating rate was 10 °C/min (CN(2)), while when 5 g of oxalic acid was used, the heating rate was 5 °C/min (CN(5)). In the second case, the heating rate had to be lower because the higher amount of oxalic acid resulted in a rapid release of gases, causing the sample to decompose completely.[22]

The plasma treated samples were obtained by dielectric barrier discharge (DBD) plasma at atmospheric pressure in air, with the configuration consisting of two plane-parallel electrodes, dimension (20.0×8.0) cm^2, covered by a 0.70 mm thick alumina layer. The sample was placed between the electrodes, where their distance was fixed with glass space holders in order to obtain a discharge gap of 3 mm and to prevent the sample from scattering outside the system. All samples were treated under the same conditions: the operating voltage was 16 kV at a frequency of 150 Hz and the treatment time was 5 min. The samples obtained were labelled as CN-pt, CN(2)-pt and CN(5)-pt.

The crystal structure and the surface chemical functional groups of the samples were characterized using an X-ray diffractometer (XRD) (Cu-Kα1,2 radiation, λ = 0.1540 nm, Rigaku SmartLab, Tokyo, Japan) at a room temperature, with 0.02° 2θ steps and 10 °/min counting time, in the 5–40° 2θ range and a Fourier transmission infrared spectrometer (FTIR), Thermo Scientific Nicolet iS10 in attenuated total reflection mode and in the wave number range of 400–4000 cm^{-1}, respectively. The morphology of the sample was characterised using field emission scanning electron microscopy, FESEM (Tescan Mira3 XMU) at a working voltage of 20 kV. To ensure the conductivity of the samples, they were previously sputter-coated with gold. An EDS analysis was performed on an INCAx-act LN2-free analytical silicon drift detector of characteristic X-rays with PentaFET® Precision and Aztec 4.3 software package (Oxford Instruments, UK) connected to a Tescan Mira3 XMU. Elemental mapping was carried out over three selected areas of dimension 50 μm ×50 μm. The UV–Vis diffuse reflectance spectra (DRS) of the samples were recorded on a Shimadzu 2600 UV–Vis spectrophotometer with integrated ISR-2600-Plus sphere and $BaSO_4$ as the standard reference. The Kubelka-Munk function given as F(R) was used to calculate the absorption spectra from the reflectance data. Photoluminescence (PL) spectra were obtained using a Fluorolog-3 FL3-221 spectrofluorometer system (Horiba Jobin-Yvon) with a 450 W xenon lamp as the excitation source and an excitation wavelength of 370 nm.

The titration method was used to study the content of acidic groups on the surface. Briefly, 100 mg of the sample was mixed with 50 ml of 0.1 M NaOH solution (Reahem d.o.o, Novi Sad (F = 0.9799)) and left in a shaker for 24 h. The powder was then separated from the supernatant by centrifugation (5 min at 6000 rpm) and the supernatant was titrated with 0.1 M HCl (Alfapanon, Serbia (F =0.9934)) solution and methyl orange as an indicator. The equation used to calculate the content of acid groups (X) is:

$$X = \frac{V_{NaOH}C_{NaOH} - V_{HCl}C_{HCl}}{m} \quad (1)$$

where V_{NaOH} and C_{NaOH} are the volume and the concentration of the NaOH solution, V_{HCl} and C_{HCl} are the volume and the concentration of the HCl solution required to reach the equilibrium point during the titration, and m is the mass of the material.

The performance of the synthesized photocatalysts was investigated using a 10 mg/l Cr(VI) solution, prepared by dissolving $K_2Cr_2O_7$ (Hemo, Belgrade (99.9 %)) in deionized water, with pH adjusted to 3 using concentrated (98 %) H_2SO_4 (Lachema, Czech Republic (98 %)). Briefly, 0.02 g of photocatalyst and 0.133 ml of citric acid solution (20 g/l, Lachner, Czech Republic (99.8 %)), used as a hole scavenger, were added to 40 ml Cr(VI) solution. The above suspension was magnetically stirred in the dark for 30 min before the irradiation to achieve adsorption-desorption equilibrium. To avoid overheating, the reactor used in the experiments had an outer jacket for circulating cooling water and the suspension was constantly stirred during the experiments, which were conducted at a room temperature. A lamp (High pressure Mercury Reprographic, Philips, 125 W) with a filter (GG400 Farbglass SCHOTT) for $\lambda > 400$ nm, *i.e.*, simulated visible (Vis) light, was used as the irradiation source, whose distance and intensity were kept constant during the experiment. The 1 ml suspension was collected after 15 min of irradiation and filtered to remove the photocatalyst. The concentration of Cr(VI) solution was measured using the characteristic absorption peak at 542 nm and 1,5-diphenylcarbazide (Sigma-Aldrich, USA (≥ 99 %)) as an indicator on a UV–Vis spectrophotometer (Shimadzu UV-1800).

RESULTS AND DISCUSSION

According to the results of the EDS analysis, pure CN naturally contains a certain amount of oxygen (Table I), mainly from the oxygen impurities in the precursors.[24] After oxygen doping with OA, the results showed that as the OA content increases, more oxygen is present in the samples. Another indication of oxygen doping is the colour of the samples, which is a much deeper brownish red for CN(5) with a higher O content. The oxygen content was increased in all samples after the plasma treatment. It can be seen that the C content was slightly altered, but a greater change occurred in the N content of the modified samples, suggesting that some nitrogen atoms were lost. This leads to the possibility that some of the N in the heptazine units has been replaced by oxygen, which has been reported previously as oxygen atoms could be introduced into CN in the form of lattice oxygen or oxygen-containing functional groups.[25,26]

TABLE I. Element content (wt. %) of CN and modified CNs

Sample	C	N	O
CN	35.2±0.47	62.8±0.30	2.00±0.17
CN-pt	35.7±0.30	60.8±0.93	3.52±0.62
CN(2)	35.3±1.19	62.0±1.16	2.63±0.03
CN(2)-pt	35.7±0.29	61.2±0.19	3.08±0.48
CN(5)	36.7±2.12	59.6±2.52	3.69±0.49
CN(5)-pt	35.0±0.38	58.5±0.71	6.55±0.50

The XRD patterns of all the CNs (Fig. 1a) showed a characteristic CN phase with two distinct diffraction peaks at ~13.1 and ~27.5°, indicating a typical tri-s--triazine structure.[12] The weak peak at 13.1° corresponds to the (100) plane formed by in-plane repetition of heptazine units with a distance between the heptazine units in the layer (*d*) of 0.68 nm. Meanwhile, the peak at 27.5° is assigned to the (002) plane, associated with the interplanar stacking of conjugated aromatic rings with a distance between the layers (*d*) of 0.326 nm, suggesting a layered structure similar to graphite.[27] After oxygen doping, the intensity of both peaks decreased with increasing OA content. The weaker intensity of the (100) peak indicates a smaller lateral size of the particles, namely a decrease in the size of the in-plane repeating heptazine unit, while the weaker and broader (002) peak indicates a decrease in the number of layers, implying a reduction in the stacking structures.[21,23,27] It has also been mentioned that oxygen doping into the CN structure affects the arrangement of the in-plane structural packing units, resulting in more disordered tri-s-triazine motifs, leading to a decrease in the intensity of the (100) peak.[28,29] Also, with the increase in OA, the position of the (002) peak was slightly shifted to a lower angle gradually, suggesting an increased interlayer distance in O-doped samples.[22] Obviously, both the intensity and the position of two significant peaks depend on the amount of OA used in the synthesis.

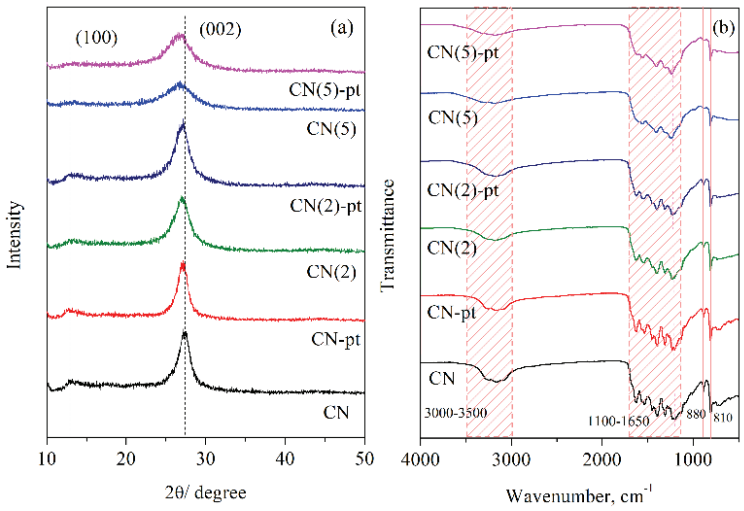

Fig. 1. a) XRD patterns and b) FTIR spectra of the CN photocatalysts.

After the plasma treatment, all samples retained a typical CN structure without any impurity phases, which means that plasma treatment doesn't affect the crystal structure of CN. Compared to pure CN, CN-pt showed no change in the intensity of the diffraction peaks, while the position of the (002) peak was

slightly shifted towards the lower values of 2θ, possibly due to nitrogen vacancies introduced during the treatment.[7,14,19] However, when the treatment was applied to the previously oxygen-doped samples, it was observed that the intensity of the (002) peak slightly increased compared to the O-doped samples, but was still lower compared to pure CN. Obviously, the plasma treatment had a different effect on the oxygen-doped samples due to the pre-existing changes in their structure.

The surface functional groups and chemical structure of the CN samples were further investigated by FTIR spectroscopy (Fig. 1b). As can be seen, all samples exhibit similar absorption bands and no significant change can be observed compared to the pure CN, which means that the oxygen doping and plasma treatment did not alter the original chemical structure of CN.[20,27] The broad band in the region 3000–3500 cm^{-1} belongs to the stretching vibrations of N–H and O–H bonds, present in the free amino groups and adsorbed water on the surface of CN. The bands in the region of 1100–1650 cm^{-1} are ascribed to the aromatic stretching vibrations of heptazine-derived units, including the C=N stretching mode and C–N out-of-plane bending vibrations.[12,27] The sharp band at approximately 810 cm^{-1} corresponds to the characteristic breathing mode of tri-s-triazine units in heterocycles and a weak peak at 880 cm^{-1} likely originates from the deformation mode of N–H in amino groups.[12,22] After the oxygen doping, it can be noticed that the intensity of the bands at 1100–1650 cm^{-1} is quite reduced, which may be the result of breaking of the triazine ring structure.[30] This can further imply that the ring opening probably occurred after introducing defects in the structure. Characteristic peaks of the C–O bond are similar to the C–N, making them difficult to detect by FTIR, but a slight shift in the position of the peak at 1198 cm^{-1} can be observed. This peak is attributed to the C–N stretching vibration and its shift to higher frequencies may indicate a transition from the C–N to the C–O bond, as these C–O vibrations appear at higher frequencies.[22,23,25] The change in intensity and shape of these bands is more significant after oxygen doping rather than after plasma treatment, so perhaps the conditions applied during the plasma treatment were not strong enough to cause some noticeable changes in the FTIR spectra, as was also shown by the XRD results. It can also be observed that the shape of broad peak at 3000–3500 cm^{-1} changed; for O-doped samples it became broader with the increase of OA and after the plasma treatment its shape did not change but the intensity was reduced.

The morphological characteristics of CN and modified samples were examined using FESEM (Fig. 2). As expected, the FESEM image of CN showed a porous structure composed of agglomerated, irregular, layered particles. After oxygen doping, it can be observed that the particles became more flaky and the irregular structure became even more porous. When a higher amount of oxalic acid was used, a more porous structure was obtained and the fragmentation of the

layers was more pronounced. Apparently, the calcination of oxalic acid and urea produced gases such as NH_3 and CO_2, which acted as bubble-forming agents. This resulted in the curling of the nanosheets and the formation of a porous structure in the samples.[14,26,28,29] Plasma treatment of the CN and O-doped samples did not make a significant difference due to the mild conditions of the DBD system, so a similar morphology was observed.

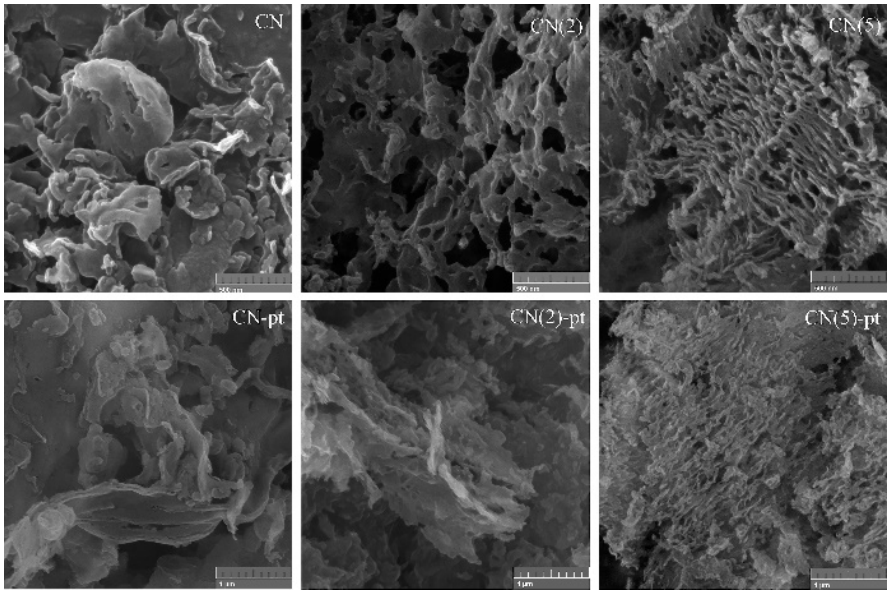

Fig. 2. FESEM photographs of the CN photocatalysts.

UV–Vis diffuse reflectance spectroscopy and photoluminescence (PL) spectroscopy were used to study the optical absorption and electronic properties (Fig. 3). As can be seen in Fig. 3a, the absorption edge of CN (λ_g) was at approximately 416 nm and the calculated band gap energy from the equation $E_g = 1240/\lambda_g$ was 2.98 eV, which is in agreement with previous reports.[3,28,31] The results showed that a significant increase in visible light absorption was observed after the inclusion of oxalic acid in the CN synthesis, with respect to the OA content. It is known that elemental doping can affect the optical properties of semiconductors and this change confirms the oxygen doping reported previously.[26,32] From the obtained DRS spectra of the O-doped samples, it can be seen that new absorption bands form between 400 and 600 nm, which has been attributed to the $n \rightarrow \pi^*$ electron transition associated with the lone pairs of the edge nitrogen atoms within the heptazine units.[33] As the two O-doped samples exhibited a significant red shift of the absorption edges, this corresponds to a decrease in band gap energies (Table II) and a higher utilization of visible light.

When plasma treated, CN-pt showed an absorption edge similar to CN, indicating that the optical band gap was not changed. It was previously reported that the band gap of CN would narrow after introducing nitrogen vacancies, but in this case the band gap remained the same, meaning that the plasma treatment didn't create this type of defect. Nevertheless, the C/N ratio was increased (Table I) and the explanation for this could be the transformation of the terminal amino groups into C–O and C=O groups as a result of treating the CN sample with plasma species.[7] Interestingly, the band gap energy was affected by plasma treatment of O-doped samples. Plasma treatment and oxygen doping of CN resulted in a synergistic narrowing of the band gap, possibly due to the introduction of oxygen atoms and the pre-existing structural modification during the doping process. A more significant shift can be observed in the CN(5)-pt sample, which was obtained with a larger amount of OA during synthesis and contains more oxygen, meaning that there are already greater changes compared to CN(2). Because of this, carboxyl groups were more easily attached during the plasma treatment, leading to the even higher oxygen content in this sample, giving it the narrowest band gap.[34]

The position of the valence and conduction bands, *i.e.*, E_{VB} and E_{CB} can be calculated using the empirical formula $E_{VB} = \chi - E_e + 0.5E_g$, where E_{VB} is the valence band potential, χ represents the electronegativity of the semiconductor (4.67 eV for CN), E_e is the energy of free electrons on the hydrogen scale (~4.5 eV), while E_g is the band gap energy of the semiconductor. Furthermore, E_{CB} can be calculated from the equation: $E_{CB} = E_{VB} - E_g$.[35–37]

TABLE II. Absorption edge, band gap energy, valence and conduction band potentials and surface acidic groups (SAG) of the CN photocatalysts

Sample	λ_g / nm	E_g / eV	E_{VB} / eV	E_{CB}/ eV	SAG groups, mmol/g
CN	416	2.98	1.66	–1.32	1.83
CN-pt	414	2.99	1.66	–1.33	6.60
CN(2)	446	2.78	1.56	–1.22	5.70
CN(2)-pt	450	2.76	1.55	–1.21	13.5
CN(5)	484	2.56	1.45	–1.11	8.40
CN(5)-pt	507	2.44	1.39	–1.05	19.5

Although the DRS results suggest that the photocatalytic activity of the obtained samples should be improved under visible irradiation, it doesn't necessarily mean that this will happen. The band gap energy was reduced, but so was the reduction potential of electrons from the conduction band, which could negatively affect the photocatalytic activity of the synthesized samples.

From Fig. 3b it can be seen that CN has a strong PL emission peak at 458 nm, while the spectra of the O-doped samples have one more peak, indicating two recombination centres.[38] The position of the new peak (at around 560 nm) is

consistent with the extended absorption range and enhanced visible light absorption, as confirmed by DRS spectra. As expected, CN-pt showed the PL peak at practically the same position as CN. PL spectroscopy was also used to evaluate the transfer and separation efficiency of photogenerated electrons and holes. The intensity of the emission peak is related to the recombination rate of charge carriers, *i.e.*, a lower emission peak means that recombination of charge carriers is suppressed due to better separation. Compared to CN, all samples had lower PL peak intensities, with the greatest suppression for CN(5). The results showed that after plasma treatment of CN, the recombination rate was reduced (sample CN-pt), but when O-doped samples were plasma treated, it led to an increase in peak intensity. It is known that the oxygen atom has more electrons than the nitrogen atom, so assuming that oxygen doping replaces nitrogen atoms, this would result in the generation of an additional electron and a further change in the electronic property of CN. It is possible that the charge density and mobility have been increased following the incorporation of oxygen atoms due to the extended delocalized π-electron system. In addition, the charge redistribution around the dopant caused an electronic polarization effect, creating an internal electric field that favoured carrier separation.[25,29] This could explain why O-CN samples showed a much lower PL peak intensity and should have a lower electron–hole pair recombination rate. However, the oxygen content was increased in CN-pt (Table I) and it showed a lower recombination rate compared to CN. It has been mentioned that plasma treatment could introduce oxygen-containing functional groups that could alter the charge distribution and attract electrons to the surface. Logically, it was expected that after plasma treatment of O-CN samples, the recombination rate of carriers would be further suppressed due to the synergistic effect of oxygen doping and higher content of oxygen-containing surface functional groups. However, the PL spectra results showed that CN(2)-pt and CN(5)--pt had higher PL emission peak intensities compared to only oxygen-doped samples. Perhaps the distribution of oxygen-containing functional groups was not homogeneous due to the presence of already modified structure, or some other defects were created which acted as recombination centers.

The content of oxygen-containing surface functional groups was also evaluated according to the content of acidic surface groups (Table II). Previous results (Table I) already confirmed that the oxygen content was increased after doping and also after plasma treatment, with the highest oxygen content being present in the CN(5)-pt. Not surprisingly, this sample also had the highest content of acidic groups on the surface. This can be explained by the fact that the previous ring opening during oxygen doping facilitates the attachment of oxygen-containing functional groups to the now more exposed ends. Although CN(5)-pt had the higher content of acidic functional groups on the surface compared to CN(5), the intensity of the PL peak decreased more in the case of CN(5). This is

of course evidence that many factors influence the intensity of the PL peak, and in this case perhaps the lower number of layers in the CN(5) particles, as confirmed by XRD.

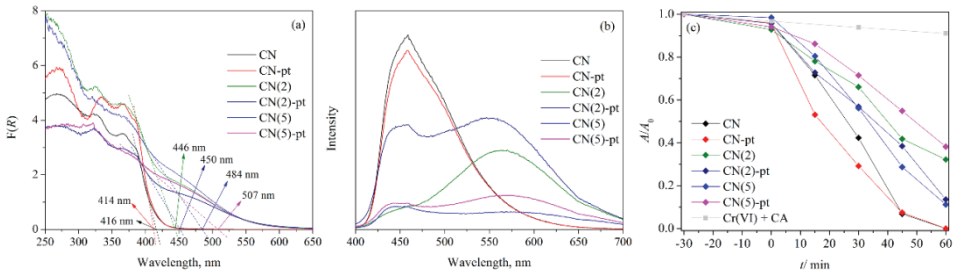

Fig. 3. The a) UV–Vis absorption spectra, b) PL emission spectra and c) photocatalytic reduction of Cr(VI) with the CN photocatalysts under visible irradiation.

In order to verify the impact of oxygen doping and plasma treatment of CN on its photocatalytic performance, the as-synthesized samples were used for a photocatalytic reduction of Cr(VI) under visible irradiation at pH 3, with citric acid (CA) serving as a hole scavenger. The acidic conditions were chosen because the reduction of Cr(VI) to Cr(III) is favoured at lower pH values. To further enhance the photocatalytic efficiency, citric acid was used as a hole scavenger to prevent re-oxidation of Cr(III) and to allow oxidation and reduction reactions to occur simultaneously. It was shown that citric acid has a low reduction potential, as evidenced by the insignificant decrease in Cr(VI) concentration in the experiment without photocatalyst (Cr(VI) + CA in Fig. 3c). Preliminary experiments showed that 30 min is sufficient time to achieve adsorption-desorption equilibrium in the dark for all samples. Fig. 3c shows very small differences in Cr(VI) concentration after 30 min in the dark, indicating that the modifications did not significantly changed the adsorption capacity for Cr(VI).

The photocatalytic reduction ability of the synthesized CNs towards Cr(VI) within 60 min was CN-pt > CN > CN(5) >CN(2)-pt > CN(2) > CN(5)-pt. Somewhat expectedly, CN-pt exhibited the best results, slightly better compared to pure CN, since its properties were quite similar to those of CN, except that the PL spectra indicated enhanced separation efficiency of the photogenerated charge carriers. It is likely that during the plasma treatment in air, various oxygen-containing functional groups were introduced (Table II), which resulted in more electrons reaching the photocatalyst surface to participate in the reduction reactions.

In contrast, the remaining samples showed reduced photocatalytic activity compared to the pristine CN. After oxygen doping, it was observed that the band gap energy of the samples decreased, implying an increase in visible light absorption (Fig. 3a). Additionally, the PL spectra suggest that the oxygen-doped samples may exhibit enhanced photocatalytic efficiency due to reduced electron-

hole recombination, but the outcome was contrary to expectations. As mentioned above, the lower intensity of the PL peaks is related to the lower recombination rate of the charge carriers, but another possible explanation for the observed reduction in PL intensity is that the lower number of e^-–h^+ pairs was generated after irradiation. This interpretation suggests that the photocatalysts will exhibit reduced photocatalytic activity under visible irradiation due to fewer electrons generated for reduction reactions at the sample surface. In addition, a narrowed band gap results in altered positions of the valence and conduction bands. In this case, this resulted in a decrease in the reduction potential of the electrons, thereby reducing the reduction capacity of the photocatalyst. The lowest photocatalytic efficiency of CN(5)-pt is in agreement with the previous statement as it has the narrowest band gap and the lowest redox capacity.

The explanation of how oxygen doping leads to the extension of the delocalized π-electron system and therefore to a better separation efficiency of the charge carriers could also be questioned here, taking into account the results of photocatalytic experiments.[25] The modification strategy that included oxygen doping was the ring structure engineering, *i.e.*, opening of the heptazine ring during the introduction of defects in order to enhance the attachment of oxygen-containing functional groups. With this in mind, it is possible that this led to the breaking of the C–N bonds, as shown by the FTIR spectra, and therefore to the reduction of the π-conjugation system rather than an expansion.

CONCLUSION

In this work, two modification strategies to introduce surface functional groups, oxygen doping and plasma treatment, were successfully applied.

Oxygen doping was evident from the colour change: dark orange of O-doped samples *versus* light yellow of pristine CN. The doping decreased crystallinity, increased porosity and reduced nitrogen content, probably due to heptazine ring opening and defect formation with oxygen atoms replacing nitrogen. This resulted in a narrower band gap and lower reduction and oxidation potentials, which were more pronounced in CN(5) than in CN(2). Mild DBD plasma increase in crystallinity and band gap narrowing, especially for CN(5).

Plasma treatment increased the oxygen content, probably by introducing oxygen-containing functional groups. In previously O-doped CN, existing defects facilitated the incorporation of new functional groups so that CN(2)-pt and especially CN(5)-pt had the highest oxygen content and acidic surface groups. However, except for CN-pt, the photocatalytic activity for Cr(VI) reduction under visible light did not improve. Although the band gap narrowing resulted in improved visible light absorption, it also resulted in a significant decrease in the reduction potential. This was obviously detrimental to the lower activity of the CN photocatalysts for Cr(VI) reduction. CN(5)-pt showed the lowest activity

under these conditions. Notably, the combination of doping and plasma treatment improved the functional group attachment and narrowed the band gap, offering potential for future optimization

Acknowledgment. The authors wish to acknowledge the financial support for this research from The Ministry of Science, Technological Development and Innovation of the Republic of Serbia through project contracts No. 451-03-65/2024-03/200135, 451-03-66/ /2024-03/200287 and 451-03-47/2023-01/200162.

И З В О Д

МОДИФИКОВАЊЕ КАРАКТЕРИСТИКА ПОВРШИНЕ И ФОТОКАТАЛИТИЧКЕ АКТИВНОСТИ ЧИСТОГ И g-C_3N_4 ДОПИРАНОГ КИСЕОНИКОМ ПОМОЋУ ПЛАЗМА ПОСТУПКА

ЈАНА Љ. ПЕТРОВИЋ[1*], ЖЕЉКО РАДОВАНОВИЋ[1], БРАТИСЛАВ ОБРАДОВИЋ[2], ЂОРЂЕ ЈАНАЋКОВИЋ[3] и РАДА ПЕТРОВИЋ[3]

[1]Иновациони центар Технолошко–металуршкоī факултета, д.о.о., Београд, [2]Универзитет у Београду, Физички факултет, Београд и [3]Универзитет у Београду, Технолошко–металуршки факултет, Београд

Графитни угљеник(IV)-нитрид (CN) представља полупроводник изграђен од неметала, који има широку примену у фотокатализи, укључујући и фотокаталитичку редукцију Cr(VI) под дејством видљивог зрачења. Како би се унапредила својства CN синтетисаног термичком полимеризацијом урее, примењене су две методе модификације: а) допирање кисеоником поступком ко-калцинације урее са две различите количине оксалне киселине, и б) плазма третман диелектричним баријерним пражњењем (енгл. *dielectric barrier discharge* (DBD)). Плазма третман је примењен на чист и на CN допиран кисеоником. За карактеризацију фотокатализатора коришћене су XRD, FTIR, FESEM, EDS, PL и DRS методе анализе, као и поступак за одређивање броја површински киселих функционалних група. Резултати су показали да је садржај кисеоника повећан у оба случаја: током допирања кисеоником долази до замене азота кисеоником у решетки, док током плазма третмана кисеоничне функционалне групе се везују на површини. Такође, плазма третманом претходно допираних узорака су функционалне групе које садрже O лакше везане због „отвореног“ хептазинског прстена. Допирање кисеоником је довело до сужавања забрањене зоне, које је било још више изражено након плазма третмана допираних узорака, при чему су смањени и оксидациони и редукциони потенцијал узорака. Иако је побољшана апсорпција видљивог зрачења, ово је допринело смањеној активности за фотокаталитичку редукцију Cr(VI). Најбољи резултати су постигнути са плазма третираним чистим CN, због повећаног садржаја функционалних група које садрже кисеоник што је допринело мањој брзини рекомбинације носилаца наелектрисања.

(Примљено 10. новембра, ревидирано 19. новембра 2024, прихваћено 10. децембра 2025)

REFERENCES

1. W. Zhu, Y. Yue, H. Wang, B. Zhang, R. Hou, J. Xiao, X. Huang, A. Ishag, Y. Sun, *J. Env. Chem. Eng.* **11** (2023) 110164 (https://doi.org/10.1016/j.jece.2023.110164)
2. M. Pourmadadi, E. Rahmani, M. M. Eshaghi, A. Shamsabadipour, S. Ghotekar, A. Rahdar, L. F. R. Ferreira, *J. Drug Deliv. Sci. Technol.* **79** (2023) 104001 (https://doi.org/10.1016/j.jddst.2022.104001)
3. J. Liang, C. Jing, J. Wang, Y. Men, *Molecules* **26** (2021) 7054 (https://doi.org/10.3390/molecules26227054)

4. M. Ismael, *J. Alloys Comp.* **846** (2020) 156446 (https://doi.org/10.1016/j.jallcom.2020.156446)
5. N. S. N. Hasnan, M. A. Mohamed, Z. A. M. Hir, *Adv. Mat. Technol.* **7** (2021) 2100993 (https://doi.org/10.1002/admt.202100993)
6. J. Gu, Y. Yu, S. Chen, W. Shi, Y. Wang, Y. Liao, H. Chen, F. Jiang, *Chem. Eng. J.* **424** (2021) 130539 (https://doi.org/10.1016/j.cej.2021.130539)
7. Z. Mao, J. Chen, Y. Yang, L. Bie, B. D. Fahlman, D. Wang, *Carbon* **123** (2017) 651 (http://dx.doi.org/10.1016/j.carbon.2017.08.020)
8. Z. Teng, N. Yang, H. Lv, S. Wang, M. Hu, C. Wang, D. Wang, G. Wang, *Chem*. **5** (2019) 664 (https://doi.org/10.1016/j.chempr.2018.12.009)
9. F. Yu, L. Wang, Q. Xing, D. Wang, X. Jiang, G. Li, A. Zheng, F. Ai, J. Zou, *Chin. Chem. Lett.* **31** (2020) 1648 (https://doi.org/10.1016/j.cclet.2019.08.020)
10. X. Bu, J. Li, S. Yang, J. Sun, Y. Deng, Y. Yang, G. Wang, Z. Peng, P. He, X. Wang, G. Ding, J. Yang, X. Xie, *ACS Appl. Mat. Interf.* **8** (2016) 31419 (https://doi.org/10.1021/acsami.6b10516)
11. Y. Li, Z. He, L. Liu, Y. Jiang, W. Ong, Y. Duan, W. Ho, F. Dong, *Nano Energy* **105** (2023) 108032 (https://doi.org/10.1016/j.nanoen.2022.108032)
12. J. Wen, J. Xie, X. Chen, X. Li, *Appl. Surf. Sci.* **391** (2017) 72 (http://dx.doi.org/10.1016/j.apsusc.2016.07.030)
13. N. Sakakibara, M. Shizuno, T. Kanazawa, K. Kato, A. Yamakata, S. Nozawa, T. Ito, K. Terashima, K. Maeda, Y. Tamaki, O. Ishitani, *ACS Appl. Mat. Interf.* **15** (2023) 13205 (https://doi.org/10.1021/acsami.3c00955)
14. N. Lu, N. Liu, Y. Hui, K. Shang, N. Jiang, J. Li, Y. Wu, *Chemosphere* **241** (2020) 124927 (https://doi.org/10.1016/j.chemosphere.2019.124927)
15. L. Khezami, P. Nguyen-Tri, W. A. Saoud, A. Bouzaza, A. E. Jery, D. D. Nguyen, V. K. Gupta, A. A. Assadi, *J. Env. Manage.* **299** (2021) 113588 (https://doi.org/10.1016/j.jenvman.2021.113588)
16. Z. Zhang, J. L. Wilson, B. R. Kitt, D. W. Flaherty, *ACS Appl. Poly. Mat.* **3** (2021) 986 (https://dx.doi.org/10.1021/acsapm.0c01270)
17. J. Zhou, T. Wei, X. An, *Phys. Chem. Chem. Phys.* **25** (2023) 1538 (https://doi.org/10.1039/D2CP04836A)
18. X. Wang, Y. Chen, M. Fu, Z. Chen, Q. Huang, *Chin. J. Catal.* **39** (2018) 1672 (https://doi.org/10.1016/S1872-2067(18)63115-8)
19. Y. Zhao, E. Wang, R. Jin, *Diam. Rel. Mat.* **94** (2019) 146 (https://doi.org/10.1016/j.diamond.2019.03.004)
20. D. Wang, Z. Zhang, S. Xu, Y. Guo, S. Kang, X. Chang, *Int. J. Mol. Sci:* **23** (2022) 7381 (https://doi.org/10.3390/ijms23137381)
21. Z. Zhang, L. Cui, Y. Zhang, L. H. Klausen, M. Chen, D. Sun, S. Xu, S. Kang, J. Shi, *Appl. Catal., B* **297** (2021) 120441 (https://doi.org/10.1016/j.apcatb.2021.120441)
22. S. Xiang, Y. Lin, T. Chang, B. Mei, Y. Liang, Z. Wang, W. Sun, C. Cai, *Chemosphere* **338** (2023) 139539 (https://doi.org/10.1016/j.chemosphere.2023.139539)
23. W. Gan, J. Guo, X. Fu, J. Jin, M. Zhang, R. Chen, C. Ding, Y. Lu, J. Li, Z. Sun, *Separ. Pur. Technol.* **317** (2023) 123791 (https://doi.org/10.1016/j.seppur.2023.123791)
24. M. Z. Rahman, K. Davey, C. B. Mullins, *Adv. Sci.* **5** (2018) 1800820 (https://doi.org/10.1002/advs.201800820)
25. P. Qiu, C. Xu, H. Chen, F. Jiang, X. Wang, R. Lu, X. Zhang, *Appl. Catal., B* **206** (2017) 319 (https://doi.org/10.1016/j.apcatb.2017.01.058)

26. Y. Wei, Y. Liu, C. Liu, X. Li, K. Song, R. Wang, W. Chen, G. Zhao, R. Liu, H. Wang, G. Shi, G. Wang, *ACS Appl. Nano Mat.* **6** (2023) 16567 (https://doi.org/10.1021/acsanm.3c02762)
27. D. Wen, Y. Su, J. Fang, D. Zheng, Y. Xu, S. Zhou, A. Meng, P. Han, C. Wong, *Nano Energy* **117** (2023) 108917 (https://doi.org/10.1016/j.nanoen.2023.108917)
28. J. Yang, Y. Liang, G. Yang, K. Wang, Z. Zeng, Z. Xiong, Y. Han, *J. Col. Interf. Sci.* **607** (2022) 1527 (https://doi.org/10.1016/j.jcis.2021.09.112)
29. S. Zhang, Y. Liu, P. Gu, R. Ma, T. Wen, G. Zhao, L. Li, Y. Ai, C. Hu, X. Wang, *Appl. Catal., B* **248** (2019) 1 (https://doi.org/10.1016/j.apcatb.2019.02.008)
30. J. Zhang, B. Xin, C. Shan, W. Zhang, D. D. Dionysiou, B. Pan, *Appl. Catal., B* **292** (2021) 120155 (https://doi.org/10.1016/j.apcatb.2021.120155)
31. A. P. Alivisatos, *Science* **271** (1996) 933 (https://doi.org/10.1126/science.271.5251.933)
32. J. Fu, B. Zhu, C. Jiang, B. Cheng, W. You, J. Yu, *Small* **13** (2017) 1603938 (https://doi.org/10.1002/smll.201603938)
33. G. Zhang, G. Li, Z. Lan, L. Lin, A. Savateev, T. Heil, S. Zafeiratos, X. Wang, M. Antonietti, *Angew. Chem. Int. Ed.* **56** (2017) 13445 (https://doi.org/10.1002/anie.201706870)
34. Z. Zhang, L. Cui, Y. Zhang, L. H. Klausen, M. Chen, D. Sun, S. Xu, S. Kang, J. Shi, *Appl. Catal., B* **297** (2021) 120441 (https://doi.org/10.1016/j.apcatb.2021.120441)
35. T. N. Xuan, D. N. Thi, Q. T. Thuong, T. N. Ngoc, K. D. Quoc, Z. Molnár, S. Mukhtar, E. Szabó-Bárdos, O. Horváth, *Molecules* **28** (2023) 7810 (https://doi.org/10.3390/molecules28237810)
36. M. Guan, D. Ma, S. Hu, Y. Chen, S. Huang, *Inorg. Chem.* **50** (2010) 800 (https://doi.org/10.1021/ic101961z)
37. M. A. Butler, D. S. Ginley, *J. Electrochem. Soc.* **125** (1978) 228 (https://doi.org/10.1149/1.2131419)
38. S. Liu, D. Li, H. Sun, H. M. Ang, M. O. Tadé, S. Wang, *J. Coll. Interf. Sci.* **468** (2016) 176 (https://doi.org/10.1016/j.jcis.2016.01.051).